Asian Journal of Chemistry; Vol. 32, No. 3 (2020), 653-658

ASIAN JOURNAL OF CHEMISTRY

https://doi.org/10.14233/ajchem.2020.22397

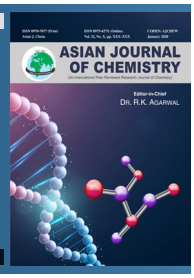

Synthesis and Characterization of Niobium Oxide Nanoparticles, Polyindole and Nb_2O_5/Polyindole Nanocomposite

S. Anandhi[1], D. Keerthika[2], M. Leo Edward[2] and V. Jaisankar[2,*]

[1]P.G. and Research Department of Chemistry, Dr. Ambedkar Government Arts College, Chennai-600039, India
[2]Department of Chemistry, Presidency College, Chennai-600005, India

*Corresponding author: E-mail: vjaisankar@gmail.com

Received: 11 August 2019; *Accepted*: 14 November 2019; *Published online*: 31 January 2019; AJC-19774

In present work, polyindole-Nb_2O_5 nanocomposite was synthesized and characterized by various analytical methods. Niobium oxide nanoparticles were prepared by sol gel method. Polyindole and Nb_2O_5 nanocomposites was prepared by chemical polymerization method and the morphology of Nb_2O_5 nanoparticles, polyindole and the nanocomposite was studied by SEM. The chemical structure of Nb_2O_5 nanoparticle, polyindole and the nanocomposite was characterized by UV-visible, FTIR and NMR spectroscopic techniques. Elemental composition and chemical character was analyzed by the use of EDAX technique. The X-ray powder diffraction technique was used to determine the degree of crystallinity and crystallite sizes. Thermal analysis such as TGA and DSC showed that the conducting polymers in the nanocomposites were stable even at high temperatures.

Keywords: Nanocomposite, Polyindole, Niobium oxide, Composites, Nanoparticles.

INTRODUCTION

Development of new materials which are having tailored surfaces are the key step towards novel technologies. In the past decades, several metal oxide such as TiO_2, ZnO_2 have been investigated and reported for its remarkable biosensor applications [1-3]. Niobium oxide is an excellent metal oxide with unique characteristics. The interest of studying Nb_2O_5 is due to its physico-chemical properties and its structural isotropy appropriate for extensive range of applications in electrochromic display, gas sensing, biosensing and photoelectrode and also in the field of microelectronics and emission display [4,5]. In these technologies, Nb_2O_5 shows a great potential and excellent properties like stability in aqueous medium, photocatalytic and redox properties [6,7]. Niobium oxide is a n-type conductor and now a days, it is used in lithium batteries as a negative electrode material [8]. Niobium oxide is a non-toxic metal oxide and hence can be used as decontaminator in water. All these properties of Nb_2O_5 are intrinsically linked to its structure. In Nb_2O_5, it is possible to regulate its structure and morphology. Depending upon the temperature, it shows a sequences of structural phases such as hexagonal (low temp), trigonal, orthorhombic (700-800 ºC) and monoclinic (850-900 ºC) [9].

Now-a-days, conducting polymers are effective coating material for the protection of metals against corrosion. Particularly, polyaniline and polypyrrole have been found to appropriately reduces the corrosion of several easily oxidizable materials [10,11]. Likewise, polyindole is an electroactive polymer having high thermal stability and great redox properties [12]. Polyindole is good choice in various domains such as organic electronics [13], electrocatalysis [14], batteries [15], anticorrosion coating [16] and sensors [17]. Its rate of degradation is very low in comparison with polyaniline and polypyrrole.

The discovery of heterogeneous hybrids, especially organic-inorganic nanocomposites today having extremely important applications. In this study, Nb_2O_5 was prepared by low temperature sol gel method and polyindole was prepared from indole monomer. Then a composite of Nb_2O_5/polyindole was synthesized by chemical polymerization technique.

The structure and morphology of Nb_2O_5 nanoparticles, polyindole and Nb_2O_5/polyindole nanocomposite were charac-

terized by means of XRD, FT-IR, UV- Visible, NMR, FE- SEM, E-DAX, TGA and DSC techniques.

EXPERIMENTAL

Commercial, $NbCl_5$ (99 %), ethanol (99 %), ammonia, hydrogen peroxide (98.9 %), ferric chloride (99 %), tartaric acid (99 %) and indole (99 %) were purchased in AR grade from Alfa Aeasar chemicals. Among these chemicals, ethanol was distilled and used. All aqueous solutions were prepared distilled water.

Synthesis of niobium oxide nanoparticles: The sol-gel method was chosen to synthesize Nb_2O_5 nanoparticles [18]. Initially, 3 g of $NbCl_5$ weighed and dissolved in ethanol (6 mL) so that a transparent yellow solution was obtained. The above $NbCl_5$ was made up with aqueous NH_3 at two different concentrations (0.5 and 0.6 mol/L). This was stirred well and niobic acid ($Nb_2O_5{\cdot}nH_2O$) was obtained. The white coloured niobic acid precipitate was centrifuged at 3000 rpm for 5 min. The obtained niobic acid was dispersed in to distilled water and centrifuged again. This same procedure was repeated for about three times. Then the precipitate was treated with 20 mL of H_2O_2. The molar ratio of H_2O_2:Nb^{5+} is 10:1. The solution was kept under cooling ice and stirred for about 5 min, a transparent yellow peroxo niobic acid sol was obtained. Then it was heated in a hot air oven at 348 K for 24 h. A 0.5 mol/L solution results a luminous yellow sol, while a 0.6 mol/L solution results a shining yellow gel without any precipitate. The sol and the gel were dried at 348 K for about 6 h in an oven. A white powder of Nb_2O_5 was obtained.

Synthesis of polyindole: In a round bottom flask, 20 mL of ethanol and 20 mmol of indole were taken and mixed together with constant stirring under nitrogen atmosphere. The purging of nitrogen was continued for about 1 h. Then, 20 mmol ferric chloride solution was added dropwise with constant stirring under 0-5 ºC and then the mixture was sonicated for 1 h. Polyindole was separated out as a greenish black precipitate. It was washed with distilled water and water soluble substances like ferric chloride and tartaric acid are washed away. A greenish black coloured polyindole powder was obtained and dried in an oven at 50-60 ºC.

Synthesis of polymer nanocomposite: Polymer nanocomposite was prepared by solution mixing method. Polyindole (1.5 g) was dissolved in 10 mL of ethanol. Nano Nb_2O_5 (15 %) was dispersed separately using magnetic stirrer. After 1 h of dispersion, nano Nb_2O_5 was added to polyindole solution. The stirring was continued for 24 h in order to get well dispersed polyindole-Nb_2O_5 nanocomposite. The product was poured into clean petri dish and the nanocomposite was kept in an oven at 50-60 ºC to remove moisture and excess solvent for 2 days.

RESULTS AND DISCUSSION

Polyindole: The FT-IR spectrum recorded for the polyindole is shown in Fig. 1a. The sharp band at 747 cm^{-1} is due to the characteristic out-of-plane deformation of the C-H bond in the benzene ring in indole molecule. The band at 1332 cm^{-1} signifies the heterocyclic ring stretching modes and 1456 cm^{-1} ascribed to characteristic stretching mode of benzene ring in polyindole [19]. The band present 1594 cm^{-1} is due to N-H deformations and the vibrations modes of C_2=C_3 aromatic bonds, typical of indoles. The band present at 1619 cm^{-1} are attributed to -C-C- stretching modes and is also indicative of highly conductive nature of polyindole. The major band appears at 3400 cm^{-1} indicates N-H stretching. The sharp band appears at about 3200 cm^{-1} for the bonded N-H stretch is absent, indicated a participation of nitrogen in polymerization [20], which is a typical characteristic band of polyindole peak.

Nb_2O_5 nanoparticles: The FT-IR spectrum recorded for N_2O_5 nanoparticles is shown in Fig. 1b. The band appears in 3600-3000 cm^{-1} region is assigned to the stretching vibration of -OH groups of the adsorbed water and niobic acid. The band at 1633 cm^{-1} is assigned to the bending vibration of H_2O molecules. The band at 1433 cm^{-1} is assigned to the stretching vibrations of the N-H bonds of NH_4^+, which corresponded to the adsorbed ions. The band around 905 cm^{-1} is assigned to the stretching vibrations of O-O bond of peroxo group (-O-O-H) [21]. The band around 658 cm^{-1} is assigned to the stretching vibration of Nb-O bond [22], which is a characteristic band of N_2O_5 nanoparticle peak.

Polyindole-Nb_2O_5 nanocomposite: The FT-IR spectrum recorded for polyindole-Nb_2O_5 nanocomposite is shown in Fig. 1c. The shifting of polyindole-Nb_2O_5 nanocomposite bands with respect to pure polyindole are because of the interaction of polyindole with the host of Nb_2O_5. A band at 1594 cm^{-1} is assigned to N-H bond vibrations in the pure polymer [23] and this band shifts to 1584 cm^{-1} in the composite. These results suggest that there are still N-H bonds in the polymer mainstay in polyindole-Nb_2O_5 nanocomposite. However, it is more disconcerted due to the polymer backbone. In the FT-IR spectra

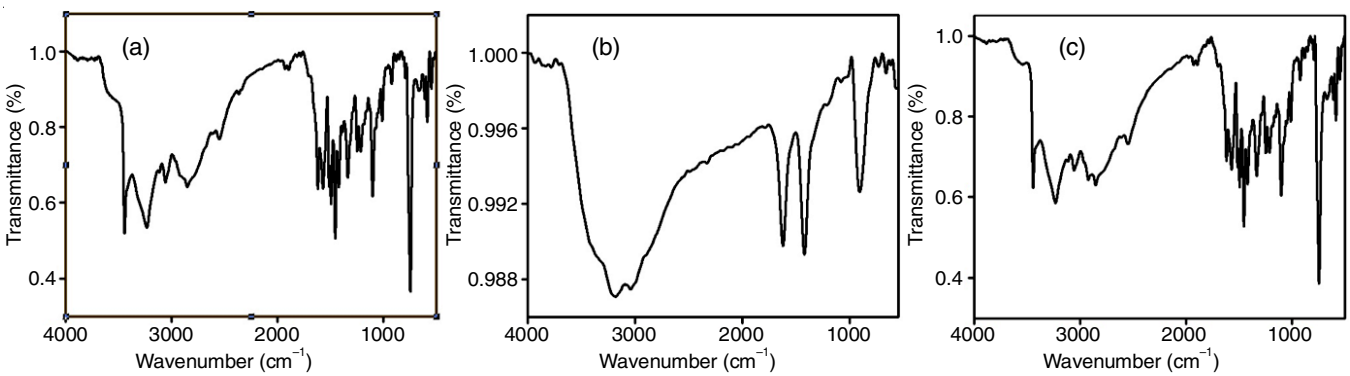

Fig. 1. FTIR spectra of (a) polyindole (b) Nb_2O_5 nanoparticles and (c) polyindole-Nb_2O_5 nanocomposite

of polyindole--Nb_2O_5 nanocomposite, peak at 1446 cm^{-1} induced by the aromatic alkene, a peak at 1330 cm^{-1} due to the stretching modes of pyrrole ring and a peak at 749 cm^{-1} due to the out-of-plane deformation of C-H bond for benzene were witnessed. A peak at 1093 cm^{-1} corresponds to the vibration mode of C-N bond. A peak at 659 cm^{-1} corresponds to the characteristic signals of Nb-O confirm the incorporation of Nb_2O_5 nanoparticles in the polyindole matrix [24]. Compared to pure polymer, the bands in nanocomposites are very strong, because of interference of Nb_2O_5 nanoparticles. The reduced intensity of the bands is attributed to the interactions among nanoparticles and polymer matrix. A considerable shift of these peaks in nanocomposites indicates a significant interaction among Nb_2O_5 nanoparticles and the polymer.

Polyindole: The UV-visible spectrum noted for the polyindole is shown in Fig. 2a. The percentage absorption is higher on the lower wavelength side which is witnessed from the plot. The UV-visible spectrum of the prepared material shows absorption in the region of 220-300 nm [25]. The two different absorption peaks at 228 and 278 nm developed due to extensive chain length spreading of polymer. Band gap energy (E_{gap}) values were obtained by linear regression of the absorption slope by extrapolating the tangent to the energy [$(E = 1240.81/\lambda)$ *versus* absorption curve. Polyindole displays a peak at 278 nm, which is because of π-π* transition. The band gap energy of polyindole value was found to be 4.4 eV [26], which is a characteristic band of polyindole peak.

Nb_2O_5 nanoparticles: The UV-visible spectrum recorded for Nb_2O_5 nanoparticles is shown in Fig. 2b. This UV spectrum gives evidence about excitation or inter band transition of nanomaterials. Band gap energy (E_{gap}) values were estimated by linear regression of the absorption slope by extrapolating the tangent to the energy. The Nb_2O_5 nanoparticle shows a signal at 292 nm, which is due to the π-π* transition [27,28]. The band gap energy of niobium pentoxide nanoparticles value is 4.2 eV, which is a characteristic band of Nb_2O_5 nanoparticle peak.

Polyindole-Nb_2O_5 nanocomposites: A UV-visible spectrum of polyindole-Nb_2O_5 nanocomposites is shown in Fig. 2c. The presence of two peaks at 214 and 278 nm in the UV-visible spectrum of polyindole indicates a formation of polyindole-Nb_2O_5 nanocomposites [29]. A peak at 278 nm corresponds to π-π* transition and the band at 278 nm is due to polymer coordinated with Nb_2O_5 nanoparticles. In the present work, Nb_2O_5 nanoparticles were incorporated in polyindole in which electrons are confined in all three spatial coordinates. Due to increased quantum confinement, these Nb_2O_5 nanoparticles exhibit new physical properties which are strongly dependent upon the nanocrystal size.

^{1}H NMR analysis: The ^{1}H NMR spectra were recorded on a Bruker Advance III 400 NMR spectrometer. Deuterium substituted dimethyl sulfoxide (CD_3SOCD_3) were used as the solvents for polymer, respectively.

The ^{1}H NMR spectrum of polyindole (Fig. 3a), the proton signals were much wider than the corresponding proton lines of indole since the extensive molar mass dispersal of polymer, which leads to slightly dissimilar surroundings of atoms. The ^{1}H chemical shifts moved to a lower field, which was mostly owing to the introduction of higher conjugation length in the polymer main chains. In Fig. 3a, there were four peaks H-4 (δ 7.63), H-5 (δ 7.02), H-6 (δ 7.08), H-7 (δ 7.42) are demonstrated with the benzene ring of polyindole units. The chemical shifts of N-H band were seen at 10.8 δ ppm [30]. These inferred that there were static N-H bonds on the polyindole backbone. So, a decision could be sensibly drawn that the N-H bonds were very stable throughout chemical oxidative polymerization, further confirming the polymerization at C_2 and C_3 site.

^{13}C NMR analysis: The ^{13}C resonances of organic compounds are found over a chemical shift range of 300 ppm compared with less than 20 ppm for protons. The proton decoupled ^{13}C NMR spectra of these polyindole have been recorded in DMSO-d_6 with as internal standard. The ^{13}C NMR spectra of polyindole showed that the signals were much wider than the corresponding signals of indole because of the extensive molar mass dispersal of polymer or the multifaceted structure of polymer, which leads to somewhat dissimilar surroundings of the atoms. The ^{13}C NMR spectra of polyindole shows peaks at C-1 (δ 123.24), C-2 (δ 103.2), C-3 (δ 127.18), C-4 (δ 121.10), C-5 (δ 122.92), C-6 (δ 119.61), C-7 (δ 111.75), C-8 (δ 136.86) [31]. The signals C-3 to C-8 (six signals) indicates the benzene ring of polyindole units [32].

X-ray diffraction analysis

Polyindole: The X-ray diffraction patterns of powder polyindole sample were recorded on Rigaku miniflex-II X-ray diffraction using Cu *K*α radiation (λ = 1.54 Å in the range 10 -70º. The pattern shows a broad hump appears at 2θ region of 18-28º and absence of well-defined peaks in Fig. 4a, evidently showed that the synthesized material is purely amorphous [33]. The XRD pattern of polyindole shows broad diffraction peaks, suggested that polyindole was amorphous. The crysta-

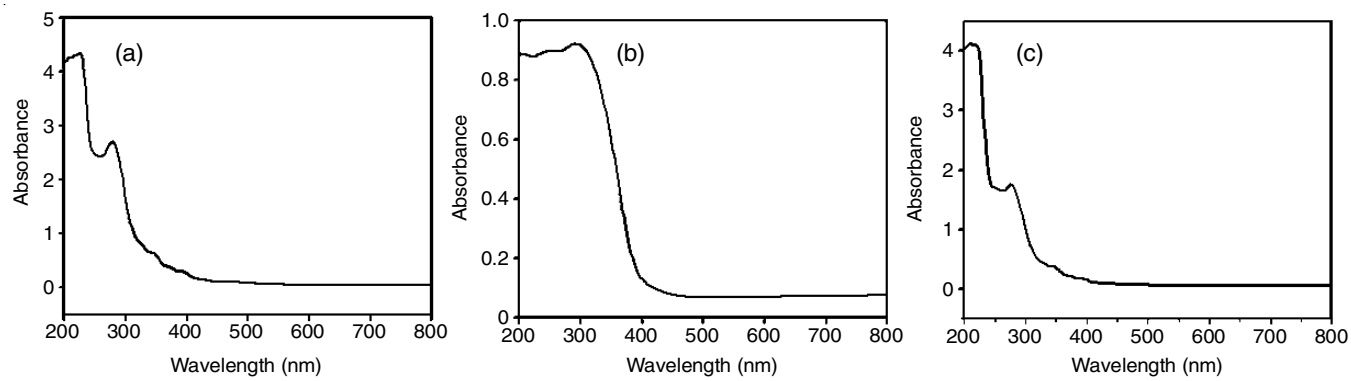

Fig. 2. UV-visible spectra of (a) polyindole (b) Nb_2O_5 nanoparticles and (c) polyindole-Nb_2O_5 nanocomposite

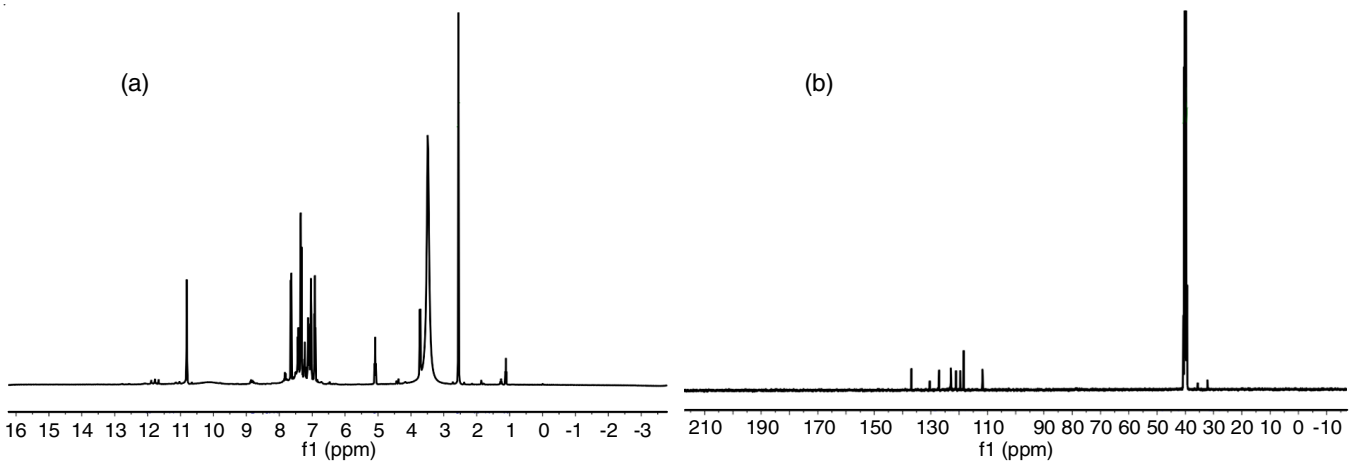

Fig. 3. (a) ^{1}H NMR and (b) ^{13}C NMR of polyindole

llite size of the powders were determined by using Scherrer′s formula:

$$D = \frac{0.9\lambda}{\beta\cos\theta}$$

where D = average crystallite size in nm, λ = wavelength of X-ray radiation, θ = Bragg′s angle and β = full width at half maximum of the peak. The particle size of polyindole is of the order of ~49 nm [25].

Nb_2O_5 nanoparticles: The X-ray diffraction patterns of the synthesized Nb_2O_5 nanoparticles are shown in Fig. 4b. To achieve the XRD patterns of the samples, [NH_3] = 0.3 mol/L was used. It was heated at 75 ºC for 24 h. A gel consisted of crystallized Nb_2O_5 nanoparticles were obtained and shows the diffuse diffraction peaks. The half width of diffraction peak of Nb_2O_5 was (001) plane. Niobium pentoxide nanoparticle′s crystallite size was found to be 3.8 nm [34].

Polyindole-Nb_2O_5 nanocomposite: The average particle size of polyindole-Nb_2O_5 nanocomposite measured through XRD using Debye-Scherrer formula is 37 nm [35]. The XRD analysis confirmed that the conducting polymer nanocomposites of polyindole began to crystallize by the incorporation of nanoparticles [17]. The XRD pattern of polyindole-Nb_2O_5 nanocomposite is shown in Fig. 4c.

SEM analysis: All the synthesized materials surface morphologies and structural topographies were studied by FE-SEM (JEOL JSM-6360).

Polyindole: The surface morphology of polyindole powder was analyzed by FE-SEM and the micrograph is presented in Fig. 5a. The macrogranular structure formed by the aggregation of small globular structures represented in the FE-SEM micrograph [36]. The nature of particles has irregular in structure, which revealed a definite amorphous morphology .The micrograph also showed the presence of aggregation, as well as an agglomeration of particles. Polyindole had an average diameter of 4.8 nm were obtained. The values are in good agreement with the values found by XRD analysis [37].

Nb_2O_5 nanoparticles: The structure of Nb_2O_5 nanoparticles consisting of even spherical particles of definite shapes and sizes around 1-2 nm (Fig. 5b). The Nb_2O_5 nanoparticles having average diameter of 4.5 nm is near to the crystallite size as calculated from the XRD pattern.

Polyindole-Nb_2O_5 nanocomposite: SEM analysis of polyindole-Nb_2O_5 nanocomposite shows a granular morphology (Fig. 5c). In this nanocomposite, Nb_2O_5 nanoparticles were dispersed and few of them were agglomerated in polyindole matrix because of the intermolecular interactions. The interaction between the materials may be strong or weak or without any chemical interactions depending upon the synthetic technique [38].

EDAX analysis: EDAX spectra of Nb_2O_5 nanoparticles and polyindole-Nb_2O_5 nanocomposite is shown in Fig. 6a and b, respectively. Compositions of Nb_2O_5 nanoparticle and polyindole-Nb_2O_5 nanocomposite are presented in Table-1.

Thermal analysis

Different scanning calorimetry (DSC) analysis of polyindole: DSC analysis of polyindole is shown in Fig. 7a. The

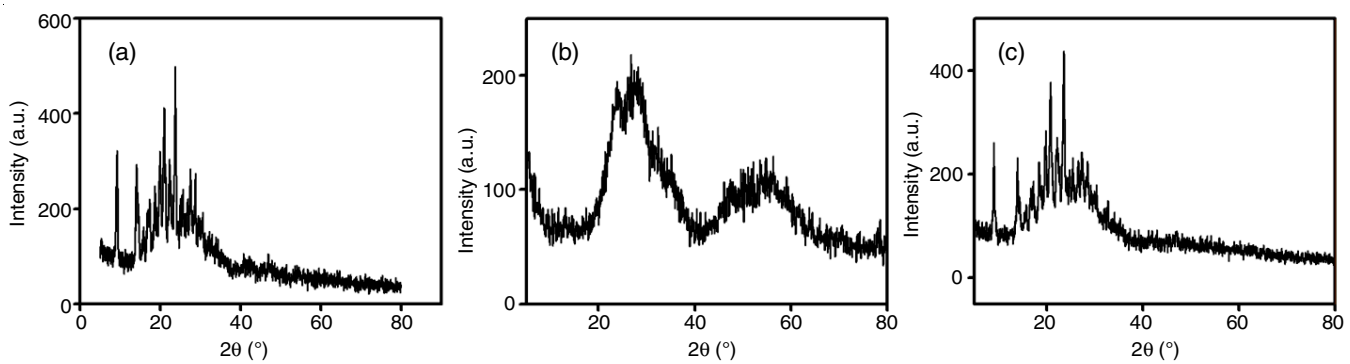

Fig. 4. XRD spectra of (a) polyindole (b) Nb_2O_5 nanoparticles and (c) polyindole-Nb_2O_5 nanocomposite

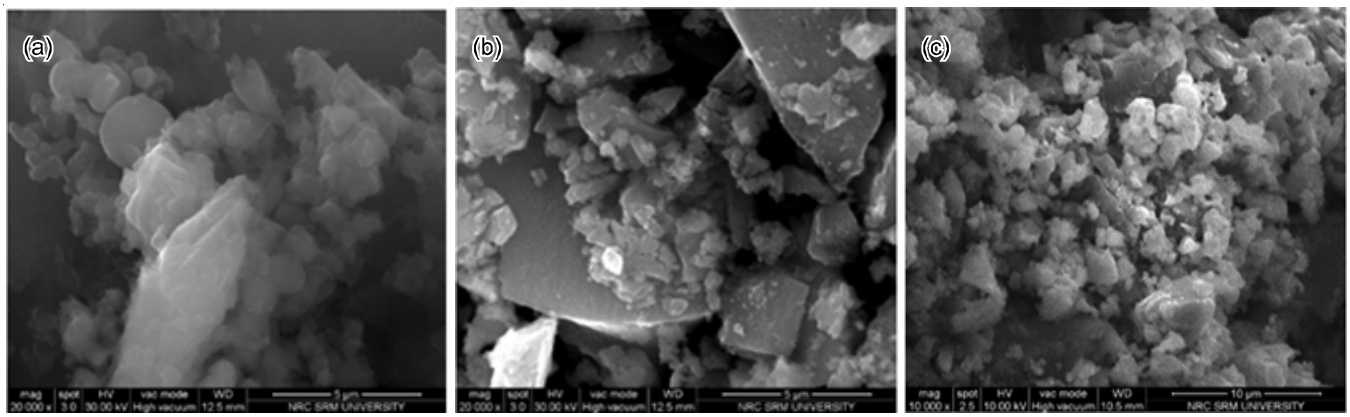

Fig. 5. FE-SEM image of (a) polyindole (b) Nb_2O_5 nanoparticles and (c) polyindole-Nb_2O_5 nanocomposite

TABLE-1
EDAX ANALYSIS OF Nb_2O_5 NANOPARTICLE AND POLYINDOLE-Nb_2O_5 NANOCOMPOSITE

Elements	Mass (%)	Mass norm	Atom abs.	Error (%)	Rel. error (%)
Nb_2O_5 nanoparticle					
Nb	54.46	79.03	39.43	1.87	3.44
O	14.41	20.92	60.57	2.94	20.39
Polyindole-Nb_2O_5 nanocomposite					
C	75.95	75.95	80.35	10.14	13.35
N	16.65	16.65	15.11	4.77	28.67
O	5.37	5.37	4.27	1.78	33.20
Nb	2.03	2.03	0.28	0.29	14.10

specimens were heated from room temperature to 800 ºC with an increment of 10 ºC/ min in air. In DSC thermogram, three endothermic peaks were found at 97.56, 178.16 and 267.05 ºC [39,40]. These peaks were due to the evaporation of water and organics. The melting point temperature of polyindole was obtained by 178.16 ºC. The glass transition and the decomposition temperatures of polyindole were observed at 97.56 ºC and 267.05 ºC, respectively.

TGA analysis of Nb_2O_5 nanoparticles: In TGA analysis, thermal behaviour of the prepared niobium oxide was studied by observing the elimination of water, *i.e.* adsorbed water in organic substances originating from ethanol and surfactants. Three key stages was witnessed. The first stage is 83.48 ºC

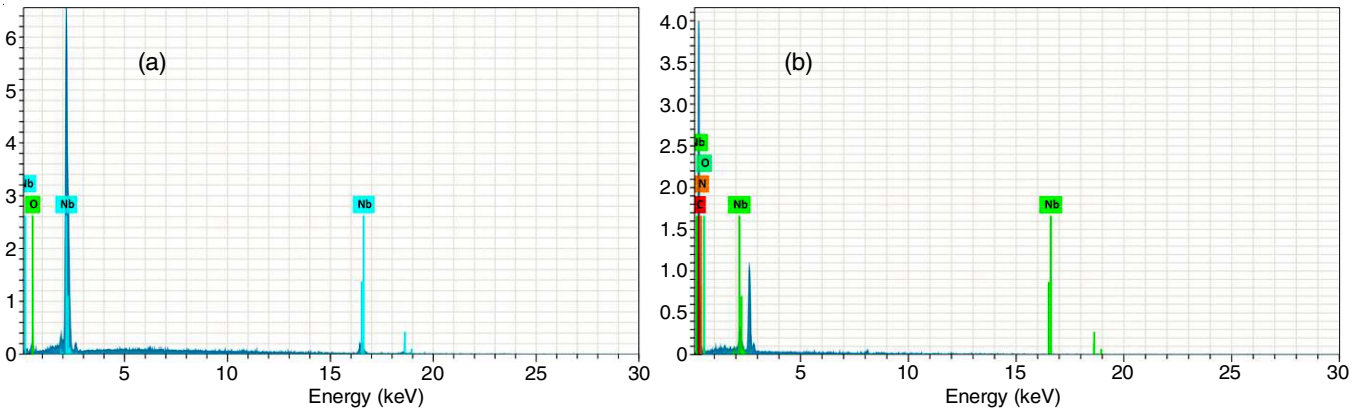

Fig. 6(a). EDAX spectra of (a) Nb_2O_5 nanoparticle and (b) polyindole-Nb_2O_5 nanocomposite

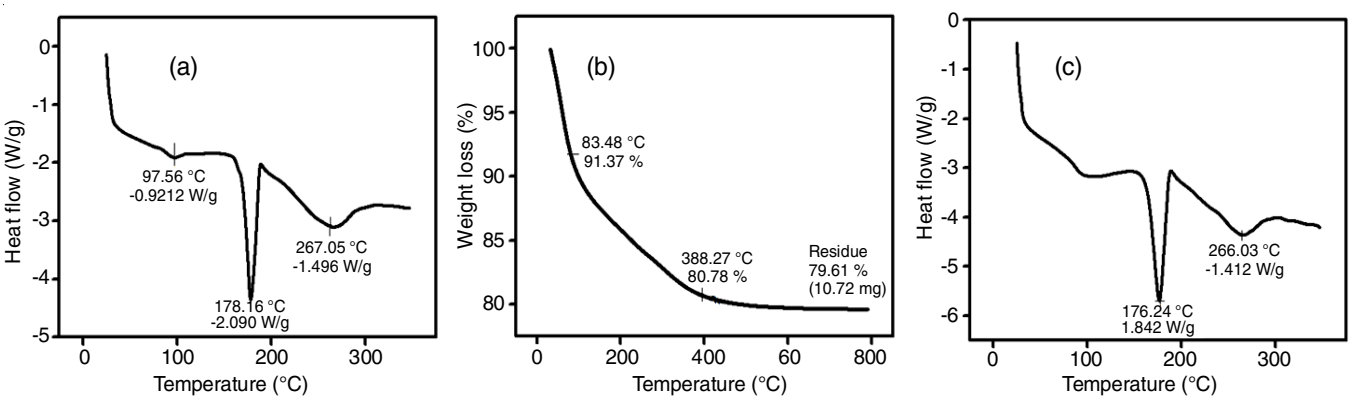

Fig. 7. (a) DSC plot of polyindole (b) TGA plot of Nb_2O_5 nanoparticles and (c) DSC plot of polyindole-Nb_2O_5 nanocomposite

region, with a 91.37 % weight loss conforming the elimination of surface water and ethanol, since sol-gel method is adapted to synthesize the sample. So organic residues are often present in samples. In the second stage, 388.27 ºC range accounted for a weight loss of 80.78 %, assigned to decomposition of organic substances, surfactant and niobium oxide and the last step is in the region of 600-800 ºC assigned to the removal of organics adsorbed on the surface and to structural arrangement of niobium oxide. Throughout the analysis, weight loss was about 91.37 % of the initial mass, with 79.61 % of the residue consisting of Nb_2O_5 (Fig. 7b).

DSC analysis of polyindole-Nb_2O_5 nanocomposite: DSC analysis of polyindole-Nb_2O_5 nanocomposite is shown in Fig. 7c. The DSC analysis of synthesized nanocomposite was obtained by endothermic peaks at 95.27,178.24 and 266 ºC [41]. The glass transition temperature of nanocomposite was observed at 95.27 ºC, melting temperature at 178.24 ºC and the decomposition temperature was observed by 266 ºC.

Conclusion

In present study, Nb_2O_5 nanoparticles, polyindole and the nanocomposites of polyindole and Nb_2O_5 were prepared. SEM images confirms that the composites are nanostructured. The chemical structures of polyindole, Nb_2O_5 nanoparticle and the nanocomposite of polyindole-Nb_2O_5 were characterized by FTIR, UV- Visible and NMR spectroscopy. The XRD technique shows the crystallite sizes were much reduced in nanocomposites of polyindole-Nb_2O_5 and additionally it confirms that composite is in amorphous state. The thermal analysis showed that the conducting polymer (polyindole) in the nanocomposites were stable even at high temperatures.

CONFLICT OF INTEREST

The authors declare that there is no conflict of interests regarding the publication of this article.

REFERENCES

1. K.-Y. Hwa and B. Subramani, *J. Biosens. Bioelectron.*, **62**, 127 (2014); https://doi.org/10.1016/j.bios.2014.06.023
2. G. Wang, X. Tan, Q. Zhou, Y. Liu, M. Wang and L. Yang, *Sens. Actuators B Chem.*, **190**, 730 (2014); https://doi.org/10.1016/j.snb.2013.09.042
3. S.-N. Ding, B.-H. Gao, D. Shan, Y.-M. Sun and S. Cosnier, *J. Biosens. Bioelectron.*, **39**, 342 (2013); https://doi.org/10.1016/j.bios.2012.07.065
4. R.A. Rani, A.S. Zoolfakar, J.Z. Ou, M.R. Field, M. Austin and K. Kalantar-zadeh, *Sens. Actuators B Chem.*, **176**, 149 (2013); https://doi.org/10.1016/j.snb.2012.09.028
5. P. Jittarporn, S. Badilescu, M.N. Al Sawafta, L. Sikong and V.-V. Truong *J. Sci. Adv. Mater. Devices*, **2**, 286 (2017); https://doi.org/10.1016/j.jsamd.2017.08.005
6. A.M. Raba, J. Bautista-Ruíz and M.R. Joya, *Mater. Res.*, **19**, 1381 (2016); https://doi.org/10.1590/1980-5373-mr-2015-0733
7. Y. Zhao, X. Zhou, L. Ye and S. Chi Edman Tsang, *J. Nano Rev. Exp.*, **3**, 17631 (2012); https://doi.org/10.3402/nano.v3i0.17631
8. N. Kumagai, I. Ishiyama and K. Tanno, *J. Power Sources*, **20**, 193 (1987); https://doi.org/10.1016/0378-7753(87)80111-8
9. M.R. Joya, J.B. Ortega, M.R.P. Angela, F.G. da Silva Filho and P. De T.C. Freire, *Metals*, **7**, 142 (2017). https://doi.org/10.3390/met7040142
10. E.B. Maarouf, D. Billaud and E. Hannecart, *Mater. Res. Bull.*, **29**, 637 (1994); https://doi.org/10.1016/0025-5408(94)90119-8
11. D. Billaud, E.B. Maarouf and E. Hannecart, *Synth. Met.*, **69**, 571 (1995); https://doi.org/10.1016/0379-6779(94)02573-H
12. P. Syed Abthagir and R. Saraswathi, *Org. Electron.*, **5**, 299 (2004); https://doi.org/10.1016/j.orgel.2004.10.002
13. W.Q. Zhou, Y. Du, H. Zhang, J. Xu and P. Yang, *Electrochim. Acta*, **55**, 2911 (2010); https://doi.org/10.1016/j.electacta.2010.01.017
14. S. Palaniappan and A. John, *J. Mol. Catal. Chem.*, **242**, 168 (2005); https://doi.org/10.1016/j.molcata.2005.07.041
15. C. Zhijiang, S. Xingjuan and F. Yanan, *J. Power Sources*, **227**, 53 (2013); https://doi.org/10.1016/j.jpowsour.2012.10.081
16. T. Tüken, M. Düdükçü, B. Yazýcý and M. Erbil, *Prog. Org. Coat.*, **50**, 273 (2004); https://doi.org/10.1016/j.porgcoat.2004.03.004
17. P.C. Pandey, *J. Chem. Soc., Faraday Trans.*, **84**, 2259 (1988); https://doi.org/10.1039/f19888402259
18. N. Uekawa, T. Kudo, F. Mori, Y.J. Wu and K. Kakegawa, *J. Colloid Interface Sci.*, **264**, 378 (2003); https://doi.org/10.1016/S0021-9797(03)00460-0
19. S.P. Koiry, V. Saxena, D. Sutar, S. Bhattacharya, D.K. Aswal, S.K. Gupta and J.V. Yakhmi, *J. Appl. Sci.*, **103**, 595 (2007); https://doi.org/10.1002/app.25245
20. Ö. Eraldemir, B. Sari, A. Gök and H. Ýbrahim Ünal, *J. Macromol. Sci. Part A Pure Appl. Chem.*, **45**, 205 (2008); https://doi.org/10.1080/10601320701839890
21. R.F. Brandao, R.L. Quirino, V.M. Mello, A.P. Tavares, A.C. Peres, F. Guinhos, J.C. Rubim and P.A.Z. Suarez, *Braz. Chem. Soc.*, **20**, 954 (2009); https://doi.org/10.1590/S0103-50532009000500022
22. C.C.M. Pereira and E.R. Lachter, *J. Appl. Catal. A, Gen.*, **266**, 67 (2004); https://doi.org/10.1016/j.apcata.2004.01.027
23. S. An, T. Abdiryim, Y. Ding and I. Nurulla, *Mater. Lett.*, **62**, 935 (2008); https://doi.org/10.1016/j.matlet.2007.07.014
24. P. Koiry, V. Saxena, D. Sutar, S. Bhattacharya, D.K. Aswal, S.K. Gupta and J.V. Yakshmi, *J. Appl. Polym. Sci*., **103**, 595 (2007); https://doi.org/10.1002/app.25245
25. N.B. Taylan, B. Sari and A.H. Unal, *J. Polym. Sci*., *B*, *Polym. Phys.*, **48**, 1290 (2010); https://doi.org/10.1002/polb.22023
26. L. Joshi and R. Prakash, *Mater. Lett.*, **65**, 3016 (2011); https://doi.org/10.1016/j.matlet.2011.06.036
27. T. Sreethawong, S. Ngamsinlapasathian and S. Yoshikawa, *Mater. Lett.*, **78**, 135 (2012); https://doi.org/10.1016/j.matlet.2012.03.045
28. H.Y. Lin, H.C. Yang and W.L. Wang, *Catal. Today*, **174**, 106 (2011); https://doi.org/10.1016/j.cattod.2011.01.052
29. G. Nie, L. Zhou and H. Yang, *J. Mater. Chem.*, **21**, 13873 (2011); https://doi.org/10.1039/C1JM11723H
30. G. Nie, X. Han, J. Hou and S. Zhang, *J. Electroanal. Chem.*, **604**, 125 (2007); https://doi.org/10.1016/j.jelechem.2007.03.010
31. M. Tiwari, A. Kumar, H.S. Umre and R. Prakash, *J. Appl. Polym. Sci.*, **132**, 42192 (2007); https://doi.org/10.1002/app.42192
32. H.E. Gottlieb, V. Kotlyar and A. Nudelman, *J. Org. Chem.*, **62**, 7512 (1997); https://doi.org/10.1021/jo971176v
33. B. Gupta, D.S. Chauhan and R. Prakash, *Mater. Chem. Phys.*, **120**, 625 (2010); https://doi.org/10.1016/j.matchemphys.2009.12.026
34. J.Z. Ou, R.A. Rani, M.-H. Ham, M.R. Field, Y. Zhang, H. Zheng, P. Reece, S. Zhuiykov, S. Sriram, M. Bhaskaran, R.B. Kaner and K. Kalantar-zadeh, *ACS Nano*, **6**, 4045 (2012); https://doi.org/10.1021/nn300408p
35. M.B.G. Costa, J.M. Jaurez, M.L. Martinez, J. Cussa and O.A. Anunziata, *Micropor. Macropor. Mater.*, **153**, 191 (2012). https://doi.org/10.1016/j.micromeso.2011.12.044
36. W.Q. Zhou, Y.K. Du, F.F. Ren, C.Y. Wang, J.K. Xu and P. Yang, *Int. J. Hydrogen Energy*, **35**, 3270 (2010); https://doi.org/10.1016/j.ijhydene.2010.01.083
37. Y. Zhao, X. Zhao, L. Ye and S.C.E. Tsang, *Nano Rev*., **3**, 17631 (2012); https://doi.org/10.3402/nano.v3i0.17631
38. H. Wang, X. Kou, J. Zhang and J. Li, *Bull. Mater. Sci.*, **31**, 97 (2008); https://doi.org/10.1007/s12034-008-0017-1
39. M.F. Kotkata, A.E. Masoud, M.B. Mohamed and E.A. Mahmoud, *Phys. E*, **41**, 640 (2009); https://doi.org/10.1016/j.physe.2008.10.019
40. B. Sari, N. Yavas, M. Makulogullari, O. Erol and H.I. Unal, *React. Funct. Polym.*, **69**, 808 (2009); https://doi.org/10.1016/j.reactfunctpolym.2009.07.002
41. P. Bajau, T.V. Sreekumar and K. Sen, *Polymer*, **42**, 1707 (2001); https://doi.org/10.1016/S0032-3861(00)00583-8